



Design and characterization of Squalene-Gusperimus nanoparticles for modulation of innate immunity

Carlos E. Navarro Chica^{a,b,*}, Bart J. de Haan^b, M.M. Faas^b, Alexandra M. Smink^b, Ligia Sierra^a, Paul de Vos^b, Betty L. López^a

^a Grupo de Investigación Ciencia de los Materiales, Instituto de Química, Facultad de Ciencias Exactas y Naturales, Universidad de Antioquia, Calle 70 No. 52-21, Medellín, Antioquia, Colombia

^b Department of Pathology and Medical Biology, Section of Immunoendocrinology, University Medical Center Groningen, University of Groningen, Hanzplein 1, EA11, 9713 GZ Groningen, The Netherlands

ARTICLE INFO

Keywords:

Squalene-Gusperimus nanoparticles
In vitro evaluation
 (RSM) response surface methodology
 Block design
 Immunosuppressant

ABSTRACT

Immunosuppressive drugs are widely used for the treatment of autoimmune diseases and to prevent rejection in organ transplantation. Gusperimus is a relatively safe immunosuppressive drug with low cytotoxicity and reversible side effects. It is highly hydrophilic and unstable. Therefore, it requires administration in high doses which increases its side effects. To overcome this, here we encapsulated gusperimus as squalene-gusperimus nanoparticles (Sq-GusNPs). These nanoparticles (NPs) were obtained from nanoassembly of the squalene gusperimus (Sq-Gus) bioconjugate in water, which was synthesized starting from squalene. The size, charge, and dispersity of the Sq-GusNPs were optimized using the response surface methodology (RSM). The colloidal stability of the Sq-GusNPs was tested using an experimental block design at different storage temperatures after preparing them at different pH conditions. Sq-GusNPs showed to be colloidally stable, non-cytotoxic, readily taken up by cells, and with an anti-inflammatory effect sustained over time. We demonstrate that gusperimus was stabilized through its conjugation with squalene and subsequent formation of NPs allowing its controlled release. Overall, the Sq-GusNPs have the potential to be used as an alternative in approaches for the treatment of different pathologies where a controlled release of gusperimus could be required.

1. Introduction

Gusperimus is a drug derived from spergualin with anti-tumoral and immunosuppressive properties (Takeuchi et al., 1981). Gusperimus exerts its immunosuppressive effect through different mechanisms. Gusperimus binds to heat shock proteins and avoid translocation of the nuclear factor- κ B (NF- κ B) to the nucleus (B.Kaufman et al., 1996) also it inhibits key molecules such as Akt kinase (Kawada et al., 2002) and deoxyhypusine synthase (Nishimura et al., 2002). During the immune response, gusperimus attenuates different cytokines such as IFN γ , IL-6, TNF α , and IL-10 (Perenyei et al., 2014). Its application has been studied for the treatment of different autoimmune diseases and it was shown to be effective during prophylactic and treatment of vasculitis, glomerulonephritis, and systemic lupus erythematosus (Perenyei et al., 2014). Because of its efficacy in suppressing autoimmunity, it has also been tested in organ transplantation. It has been shown to support the

survival of grafts in both experimental animal and clinical studies in allogenic and xenogeneic settings. In neovascularized graft transplants such as skin, thyroid, pancreatic islets, as well as in transplantation of immediately vascularized organs such as kidneys, liver, pancreas, and heart gusperimus has shown to prolong graft survival and prevent rejection (Perenyei et al., 2014).

Gusperimus is a highly hydrophilic drug according to the United States Pharmacopeia (USP) as it has a solubility higher than 100 mg/mL in water ("Gusperimus | C17H37N7O3 - PubChem," n.d.). Hydrophilic drugs are often subject to low intracellular absorption, enzymatic degradation, rapid elimination, distribution below optimal levels, resistance development, poor pharmacokinetics, and low therapeutic index (Arpicco et al., 2016). Gusperimus is in addition to this chemically unstable (Fujii et al., 1989) and as a consequence is characterized as a drug with low oral bioavailability. Therefore, it needs to be administered intravenously or subcutaneously to avoid too much loss of

* Corresponding author at: Pathology and Medical Biology, Section of Immunoendocrinology, University of Groningen, University Medical Center Groningen, Hanzplein 1, EA11, 9713 GZ Groningen, the Netherlands.

E-mail address: c.e.navarro.chica@umcg.nl (C.E. Navarro Chica).

<https://doi.org/10.1016/j.ijpharm.2020.119893>

Received 25 May 2020; Received in revised form 12 July 2020; Accepted 14 September 2020

Available online 19 September 2020

0378-5173/© 2020 Elsevier B.V. All rights reserved.

bioactivity (Perenyi et al., 2014). The entrapment of hydrophilic drugs in colloidal delivery systems can in many cases overcome issues associated with stability or off-target toxicity and facilitate their use (Arpicco et al., 2016; Desmaële et al., 2012). Encapsulation in colloidal systems can improve pharmacokinetics, protect the active substance against degradation *in vivo*, maintain drug release over time, reduce side effects, and, most importantly, increase patient comfort and applicability. There are several systems available for entrapment of hydrophilic drugs including liposomes, lipid NPs, polymer NPs, mesoporous silica NPs, nanobubbles, and squalene-derived NPs (Arpicco et al., 2016). The squalene-derived NPs are produced after binding squalene covalently to the active principle obtaining a conjugate or prodrug that spontaneously self-assemble as NPs in an aqueous medium (Couvreur et al., 2006). This has several advantages over the other systems, such as the potential for high drug loading (Desmaële et al., 2012). Also, the covalent binding enhances half-life time and therewith the drug stability, which avoids “burst” release and allows fine-tuned controlled release. Finally, the lipophilic properties of squalene can enhance the affinity of the bioconjugate to cell membranes resulting in a higher drug concentration within cells, enhancing the pharmacological activity of the active principle (Feng et al., 2017).

In this study, we designed and characterized Sq-GusNPs by binding squalene covalently to gusperimus, to be used as a gusperimus controlled release system that maintains its immunosuppressive properties over time. Sq-GusNPs were designed by applying a bottom-up approach (Zhao et al., 2011) in which NPs are obtained starting from the molecular units. From squalene and through different synthesis steps the Sq-Gus bioconjugate was obtained. The characterization of the different synthesis products was performed through the analysis of Fourier transformed infrared spectroscopy (FTIR) and nuclear magnetic resonance spectroscopy (NMR) data. The use of the nanoprecipitation method and a response surface methodology (RSM) design allowed obtaining the Sq-GusNPs. The Sq-GusNPs were characterized by dynamic light scattering (DLS), transmission electron microscopy (TEM), and Z potential (ζ) measurements. The colloidal stability of the Sq-GusNPs over time was tested using a block design at three different pH values. Finally, the *in vitro* activity of Sq-GusNPs was studied using the U-937 cell line through the determination of its uptake, cytotoxicity, and anti-inflammatory capacity.

2. Materials and methods

2.1. Materials

Squalene 98%, tetrahydrofuran (THF), N-bromosuccinimide (NBS), diethyl ether (DE), sodium chloride (NaCl), sodium sulfate (Na_2SO_4), periodic acid (H_5IO_6), silver nitrate (AgNO_3), sodium hydroxide (NaOH), hydrochloric acid 37% (HCl), ethyl acetate (EA), dimethylformamide (DMF), Silica gel 60 (0.040–0.063 mm) for column chromatography (230–400 mesh ASTM), and absolute ethanol (EtOH) were purchased from Merck (Lyon, France). Petroleum ether (PE), methanol (MeOH), and hexane (Hex) were purchased from Avantor (Radnor, PA, USA). Potassium carbonate (K_2CO_3), N-hydroxysuccinimide (NHS), N,N'-dicyclohexylcarbodiimide (DCC), Nile Red, 3,3'-dihydroxyloxycarbonyl iodide (DiOC_6), propidium iodide (PI), phorbol 12-myristate 13-acetate (PMA), and lipopolysaccharides (LPS) from *Escherichia coli* O111:B4 purified by phenol extraction was purchased from Sigma-Aldrich (St. Louis, MO, USA). Gusperimus was obtained from Nordic Pharma SAS (Paris, France). Dichloromethane (DCM), and triethylamine (TEA) were purchased from Panreac (Darmstadt, Germany). The alamarBlue™ reagent was purchased from Life Technologies Europe BV (Bleiswijk, The Netherlands), and ELISA Duo-Set for human IL-10 and TNF α were purchased from R&D systems (Abingdon, United Kingdom).

2.2. Synthesis of Sq-Gus bioconjugate

Sq-Gus bioconjugate synthesis started from squalene according to the methodology proposed by Ceruti et al. (Ceruti et al., 1987) until obtaining the aldehyde derived from squalene 1,1',2-tris-nor-squalene aldehyde. Briefly, a 0.4 M solution of squalene reagent in THF was prepared and deionized water was added drop by drop under stirring until the solution became opalescent, after which THF was added until the solution turned clear again. To this solution, NBS in a molar ratio 1:1 respect to squalene was added and after stirring at room temperature for 1-hour, deionized water was added to form two phases. The organic phase was extracted with PE, washed with brine, dried with Na_2SO_4 , and subjected to rotary evaporation. From this, squalene monobromohydrin (Sq-MBH) as a pale-yellow oil was recovered by flash chromatography using as eluent PE (100%) and DE (100%). The Sq-MBH was added to a 0.3 M methanolic solution of K_2CO_3 in a molar ratio 1:1.20 (Sq-MBH: K_2CO_3), under stirring, and left for two hours at room temperature. Afterward, the reaction mixture was diluted with water, and the organic phase extracted with PE, washed with brine, dried with Na_2SO_4 and the PE evaporated under reduced pressure to obtain squalene epoxide (Sq-Ep). The Sq-Ep was added to a 0.5 M solution of H_5IO_6 in THF in a molar ratio of 1:5 (Sq-Ep: H_5IO_6) under stirring and left reacting for 15 min after which deionized water was added. The organic phase was extracted with PE, washed with brine, dried with Na_2SO_4 and the PE evaporated under reduced pressure. The concentrated extract was subjected to flash chromatography using PE/DE (95/5) as eluent, to obtain 1,1',2-tris-nor-squalene aldehyde (Sq-Ald).

Sq-Ald was subsequently transformed to 1,1',2-tris-nor-squalene acid (Sq-COOH) through an oxidation reaction following the methodology proposed by Sen and Prestwich (Sen and Prestwich, 1989). From the carboxylic acid derivative, the squalenoyl N-hydroxysuccinimidyl ester (Sq-COO-NHS) was obtained through reaction with NHS. The Sq-Gus bioconjugate was obtained from a reaction of Sq-COO-NHS with gusperimus (COUVREUR et al., 2009). To prepare the carboxylic acid derivative, a 0.076 M solution of Sq-Ald at 0 °C reacted with silver oxide (Ag_2O), which was generated in situ by addition of an aqueous solution 0.3 M of AgNO_3 in a molar ratio 1:1 (Sq-Ald: AgNO_3) and the same volume of 1.4 M NaOH solution. The reaction mixture was left under stirring for 8 h at room temperature, after which it was filtered, the pH adjusted to 1 with HCl and then the acid derivative was extracted with DE. The DE concentrated extract (after DE evaporation under reduced pressure), was subjected to flash chromatography using as eluent EA/Hex (20/80) obtaining the Sq-COOH. To prepare the Sq-COO-NHS, a 0.06 M solution of Sq-COOH in DCM reacted with NHS and DCC, both in a molar ratio of 2:1 respect to Sq-COOH. The reaction was left under stirring for two hours. Afterward, the mixture was filtered, diluted with EA, stirred for 30 min and the concentrated extract containing the Sq-COO-NHS was obtained by evaporating under reduced pressure. Finally, 2 mL of a gusperimus solution 0.01 M in dry DMF was added to 2 mL of Sq-COO-NHS solution in dry DMF in a molar ratio of 6:1 (Sq-COO-NHS:Gus), followed by addition of 20 μL of TEA. The reaction was left under stirring for 2 h. The reaction mixture was filtered and the Sq-Gus bioconjugate extracted with 20 mL of DCM, after which the aqueous phase was saturated with salt and the extraction step repeated. The extract was concentrated by reduced pressure and after flash chromatography, using as eluent DCM/EtOH 90/10 and EtOH/TEA 95/5, the Sq-Gus bioconjugate, as a solid, was obtained.

2.2.1. Fourier-Transform Infrared spectroscopy (FTIR)

Characterization for all synthesis products was carried out through FTIR using a Spectrum One FT-IR Spectrometer (PerkinElmer, Waltham, MA, USA), dispersing the samples in KBr cells with 32 scans, a resolution of 4 cm^{-1} , and a wavelength range of 4000 cm^{-1} to 450 cm^{-1} .

2.2.2. Nuclear magnetic resonance (NMR)

NMR spectra of ^1H and ^{13}C were obtained using a Bruker Ascend III

HD 600 MHz spectrometer with 5 mm cryoprobe - TCI and a Bruker Avance NEO 600 MHz spectrometer with 5 mm CryoProbe Prodigy BBO (Bruker, USA). NMR analyses were only conducted on reaction products that were obtained through a prior purification by flash chromatography. NMR data were analyzed using MestReNova software version 12. Conditions for NMR analysis are described in detail in the [supplementary information](#).

2.3. Nanoparticle preparation

2.3.1. Sq-GusNPs preparation

Sq-GusNPs were prepared through the nanoprecipitation method (Barreras-Urbina et al., 2016). For this, the pure Sq-Gus bioconjugate, obtained as previously described in section 2.2, was dissolved in absolute EtOH at a concentration of 2 mg/mL. Later 380 μ L of the previous solution was added drop by drop to 1 mL of deionized water under stirring (500 rpm) for 10 min after which EtOH was evaporated using a rotary evaporator obtaining an aqueous suspension of pure NPs. No additional components e.g. surfactants were used in nanoparticle preparation and the aqueous nanoparticle suspension was used directly for further experiments. The prepared NPs suspension was stored at 4 °C and used until 1 month after its preparation.

2.3.2. Nile red labeled Sq-GusNPs preparation

To obtain labeled Sq-GusNPs an ethanolic solution of Nile Red at a concentration of 0.1 mg/mL was prepared. From this 380 μ L was taken and EtOH was evaporated using a rotary evaporator to obtain dried crystals of Nile Red. Later 380 μ L of Sq-Gus bioconjugate dissolved in EtOH at a concentration of 2 mg/mL was added to the dried Nile Red crystals, vortexed, and NPs obtained as described in the previous section (2.3.1). The aqueous suspension of labeled Sq-GusNPs was filtered through a 0.22 μ m filter to separate the Nile red precipitate after ethanol evaporation obtaining a translucent suspension of labeled Sq-GusNPs. The prepared NPs suspension was stored at 4 °C and used until 1 month after its preparation.

2.3.3. Response surface methodology (RSM)

Conditions for nanoparticle preparation were obtained through an experimental design using the RSM in which three experimental factors were evaluated: volume of bioconjugate solution dissolved in EtOH (Vol. bioconjugate, μ L), water volume (Vol. water, mL) which is added to the bioconjugate solution, and stirring speed (stirring speed, rpm) at which the NPs are obtained (Table 1). Response variables evaluated for the RSM design were size (nm), ζ (mV), and dispersity (\bar{D}). The size was measured through DLS using a particle size analyzer HORIBA LB-550 (HORIBA, Kyoto, Japan), ζ was measured using a Zetasizer Nano Series – Nano Z (Malvern Instruments, Grovewood Road, UK), and \bar{D} was determined from size measurements according to its definition as the standard deviation (SD) of the particle diameter distribution divided by the mean particle diameter to the 2 power ($\bar{D}=(SD/Mean)^2$) (Clayton et al., 2016). The experimental design created through the RSM was a central composite design (CCD) in which the lower and upper levels indicated in Table 1 were used. The experiment was completely randomized, rotatable, and consisted of 17 treatments which included 3 central points.

Table 1

Factors and response variables evaluated in the RSM design for Sq-GusNPs obtention.

Factor	Unit	Level		Response variable	Unit
		Lower	Upper		
Vol. Bioconjugate	μ L	300	500	Size	nm
Vol. Water	mL	2	5	ζ	mV
Stirring speed	rpm	270	800	\bar{D}	

2.4. Transmission electron microscopy (TEM)

The morphology of the NPs was examined by TEM using two different methods for sample preparation. Cryo-TEM and staining were done using a FEI Tecnai T20 cryo-electron microscope equipped with a Gatan model 626 cryo-stage operating at 200 keV. For both methods, the sample was prepared depositing 2 μ L of Sq-GusNPs suspension at a concentration of 0.76 mg/mL in a holey carbon-coated grid (Quantifoil 3.5/1, Quantifoil Micro Tools, Jena, Germany). For Cryo-TEM after blotting the excess of liquid, the sample was vitrified in liquid ethane (Vitrobot, FEI, Eindhoven, The Netherlands) and transferred to the TEM microscope. For staining the excess of liquid was removed with a blotting filter paper, after a drop of 2% uranyl acetate solution was added and blotted again to remove the excess of the solution, finally, the sample was transferred to the TEM microscope.

2.5. Colloidal stability of Sq-GusNPs

Colloidal stability of Sq-GusNPs was evaluated through a block experimental design in which the time evaluated between 0 and 30 days in 11 blocks was taken as a blocking factor. The size and ζ continually were measured during the first five days as of day 0, followed by measurements every 5 days until day 30. The experimental factor for this design was the pH, which was evaluated at 3 different values 4.5, 7.4, and 9.0. These pH values were established by adding NaOH or HCl solutions to the water used for obtaining Sq-GusNPs. The experiment was carried out at two storage temperatures i.e. 4 °C and 25 °C. It was randomized, and for each temperature, this consisted of two replicas per block with a total of 66 runs.

2.6. In vitro evaluation of the functionality of Sq-GusNPs

2.6.1. Flow cytometry

Flow cytometry was carried out using the Flow cytometer BD FACSVerse (BD Biosciences, Breda, The Netherlands) counting 10,000 events for sample using a 488 nm probe for excitation and a 586/42 nm probe for emission in the cellular uptake assay for Nile Red, and a 527/32 nm and 586/42 nm probes for emission were used for DiOC₆ and PI respectively in the cytotoxicity assay. Data analysis was performed using the software FlowJo version 10.6.1.

2.6.2. Cellular uptake

To demonstrate cellular uptake of Sq-GusNPs we applied the human monocyte U-937 cell line (ATCC® CRL1593.2™) (Cell culture is described in detail in the [supporting information](#)). To this end, Sq-GusNPs labeled with the fluorescent agent Nile Red (Sq-Gus-R) were prepared as described in Section 2.3.2.

Sq-Gus-R at three different concentrations (Sq-Gus-R 1x/2x/4x) were cultured with cells in a density of 2×10^5 cells/well in 24 well plates for three hours at 37 °C and 5% CO₂. Used concentrations of Sq-GusNPs were equivalent to 2.8 μ g/mL, 5.6 μ g/mL (double concentration), and 11.2 μ g/mL (fourfold concentration) of pure gusperimus for Sq-Gus-R 1x, Sq-Gus-R 2x, and Sq-Gus-R 4x respectively. After the three hours culture period, cells were washed with plain medium and its fluorescence was measured by flow cytometry (the gating strategy is described in Fig. S1 of the [supplementary information](#)).

To discard any interference in the obtained response, four controls were used in these experiments, which were Sq-GusNPs without Nile Red to the highest used concentration (Sq-Gus 4x), Sq-GusNPs labeled with Nile Red to the highest concentration (Sq-Gus-R 4x), cells without NPs (Cs), and cells with Sq-GusNPs at the highest concentration without Nile Red (Cs + Sq-Gus 4x).

Cellular uptake was also confirmed using the fluorescence microscope EVOS® FL Cell Imaging System (Thermo Fisher Scientific, Landsmeer, The Netherlands). For this, cells were cultured with the highest concentration of Sq-GusNPs (Cs + Sq-Gus 4x), Sq-GusNPs

labeled with Nile Red (Cs + Sq-Gus-R 4x) and cells without NPs (Cs) for 3 h. Finally, cells were washed with plain medium and observed using bright light and fluorescence light with the filter EVOS™ LED Cube, CY®5.

2.6.3. Cytotoxicity

Cytotoxicity of Sq-GusNPs was measured through flow cytometry in U-937 monocytes using two viability fluorophores: DiOC₆ as an indicator of mitochondrial damage and apoptosis (Shapiro, 2000; Wang et al., 2006) and PI as an indicator of cytoplasmic membrane damage (Rosenberg et al., 2019). The use of DiOC₆ allows the detection of cells with mitochondrial damage in the early stage of apoptosis which cannot be detected with PI (Odaka et al., 1998). Briefly, 2×10^5 cells/well in 24 well plates were treated with three different concentrations of Sq-GusNPs, free gusperimus (at the same equivalent concentrations used for gusperimus previously), and free squalene as NPs (SqNPs, see [supplementary information](#) for SqNPs preparation). After treatment for 24 and 48 h, the fluorescence was measured through flow cytometry culturing the cells for 20 min with both fluorophores at a concentration of 0.06 µg/mL for DiOC₆ and 1 µg/mL for PI (the gating strategy is described in [Fig. S2](#) of the [supplementary information](#)).

2.6.4. ELISA

A sandwich ELISA (DuoSet ELISA R&D systems) for human IL-10 and TNFα were performed according to the manufacturer's instructions using the microplate spectrophotometer Benchmark Plus BIO-RAD at 450 nm with correction at 540 nm.

2.6.5. Anti-inflammatory capacity determination assay

The anti-inflammatory capacity of Sq-GusNPs was tested as follows: Human U-937 monocytes at a density of 5×10^5 cells/well in 24-well plates were differentiated into macrophages by adding PMA at a concentration of 200 nM (Haque et al., 2019). After 24 h, cells were washed with plain medium and treated with the highest concentration used in the previous experiments which was equivalent to 11.2 µg/mL of free gusperimus and 11.1 µg/mL of free squalene supplied as NPs (SqNPs) (Sq-Gus 4x, Sq 4x, and Gus 4x). This concentration was chosen since it showed an enhanced effect on cytokine downregulation at 6 h after LPS stimulation (see [Fig. S3](#) of the [supplementary information](#)). After two hours incubation, LPS (1 µg/mL) was added to stimulate inflammatory responses and IL-10 (an anti-inflammatory cytokine) and TNFα (a pro-inflammatory cytokine) production were quantified in the supernatant 6, 24, 48, 72, and 96 hours later through ELISA. Cells without any treatment served as negative control while cells treated only with LPS served as the positive control. To exclude that the observed effect in cytokine production was due to cell death, viability was measured with alamarBlue™ for exposition times between 24 and 96 h (see [Fig. S4](#) of the [supplementary information](#)).

2.6.6. Cell viability with alamarBlue™

To determine cell viability with alamarBlue™ the reagent was diluted in culture medium (10% v/v). After treatment of the cells, at 24, 48, 72, and 96 hours supernatants were collected for cytokine determination. Cells were washed with plain medium and incubated for four hours with the diluted reagent. The absorbance was measured at 570 nm with correction at 600 nm with the microplate spectrophotometer Benchmark Plus BIO-RAD (Bio-Rad Laboratories B.V, Veenendaal, The Netherlands). Cell viability was determined respect to the controls without any treatment (Cs) for each evaluated timepoint taking as 100% of viability the absorbance value for these controls.

2.7. Statistics

For the RSM and block designs the experimental design, analysis of data, and determination of optimal conditions were performed using STATGRAPHICS Centurion XVI software, Version 16.0.07 (StatPoint

Technologies Inc., USA). The experiments with cells were repeated at least 3 times and statistical analysis was carried out in GraphPad Prism, Version 8.2.0 (GraphPad Software Inc., USA). The normal distribution of data was confirmed using the D'Agostino-Pearson omnibus (K2) test. Comparisons were made using one-way ANOVA with Dunnett's post hoc test or two-way ANOVA with Tukey's post hoc test. A *p*-value < 0.05 was considered statistically significant. Results are expressed as mean ± standard deviation (SD).

3. Results

3.1. Preparation and characterization of Sq-Gus bioconjugate

The synthesis of the Sq-Gus bioconjugate involved several reaction steps with different intermediate products, which were identified by FTIR and NMR after their purification by flash chromatography. [Fig. 1](#) shows the reaction steps with the respective yields. The reaction starts with the electrophilic addition of Br in one of the external olefinic bonds of squalene (1), followed by subsequent incorporation of an OH group through a nucleophilic water attack (Clayden et al., 2012) forming the Sq-MBH (2). After obtaining Sq-MBH, bromine is displaced following a S_N2 mechanism in basic medium to produce Sq-Ep (3) (Clayden et al., 2012). This compound is transformed to Sq-Ald (4) through a reaction in which a cyclic intermediary with the periodic acid affords the epoxide cleavage (Nagarkatti and Ashley, 1973). Sq-COOH (5) is obtained as a result of the Sq-Ald oxidation by in situ formation of Ag₂O (Sen and Prestwich, 1989). From the reaction of Sq-COOH with NHS, using the coupling reagent DCC, the intermediary product Sq-COO-NHS (6) is obtained, which provides an active leaving group and reacts with gusperimus through its amine primary group for the obtaining of Sq-Gus bioconjugate (7), ("Conversion of Carboxylic acids to amides using DCC as an activating agent - Chemistry LibreTexts," n.d.).

3.1.1. FTIR characterization

The presence of characteristic functional groups of the Sq-Gus bioconjugate and the intermediary products was confirmed by FTIR and their chemical structure by NMR. [Fig. 2](#) shows the FTIR spectra of the different compounds involved in the synthesis of the Sq-Gus bioconjugate. For Sq-MBH, it is observed the presence of bands at 3470 cm⁻¹ and 633 cm⁻¹, associated with the stretching of the OH and C-Br bonds respectively (Silverstein et al., 2005). Two bands are observed for Sq-EP that correspond to the epoxide ring breathing at 1249 and 1124 cm⁻¹, as well as bands at 899 and 873 cm⁻¹ corresponding respectively to asymmetric and symmetric deformations (Ceruti et al., 1992). For Sq-Ald and Sq-COOH, stretches for the carbonyl groups bands appear at 1729 cm⁻¹ and 1711 cm⁻¹ respectively. In the case of Sq-COO-NHS, three bands are observed at 1744 cm⁻¹, 1788 cm⁻¹, and 1818 cm⁻¹ which are associated with the stretching of three different carbonyl groups in this molecule. The FTIR spectrum of Sq-Gus bioconjugate ([Fig. 2B](#)) clearly presents the bands associated with its functional groups: at 3447 cm⁻¹ the O-H stretching band; between 3050 cm⁻¹ and 2830 cm⁻¹ the C-H alkene and alkane stretching bands, respectively; and between 1600 cm⁻¹ and 1750 cm⁻¹ the bands associated with the presence of the carbonyl bonds of the secondary amide groups of this molecule (Silverstein et al., 2005). The bands between 2400 cm⁻¹ and 2800 cm⁻¹ are associated with the presence of the guanidine group of gusperimus moiety, which exhibits in this regions stretching vibrations corresponding to C-N, C=N, and N-H bonds, as it happens in molecules that contain the guanidine group such as arginine (Ebrahiminezhad et al., 2012) and the guanidine-derived salt GULAS (Thangaraj et al., 2017).

3.1.2. NMR characterization

[Fig. 3](#) shows the ¹H and ¹³C NMR spectra of the compounds involved in the synthesis of the Sq-Gus bioconjugate, for which a previous purification process by flash chromatography was done. The ¹H NMR spectra

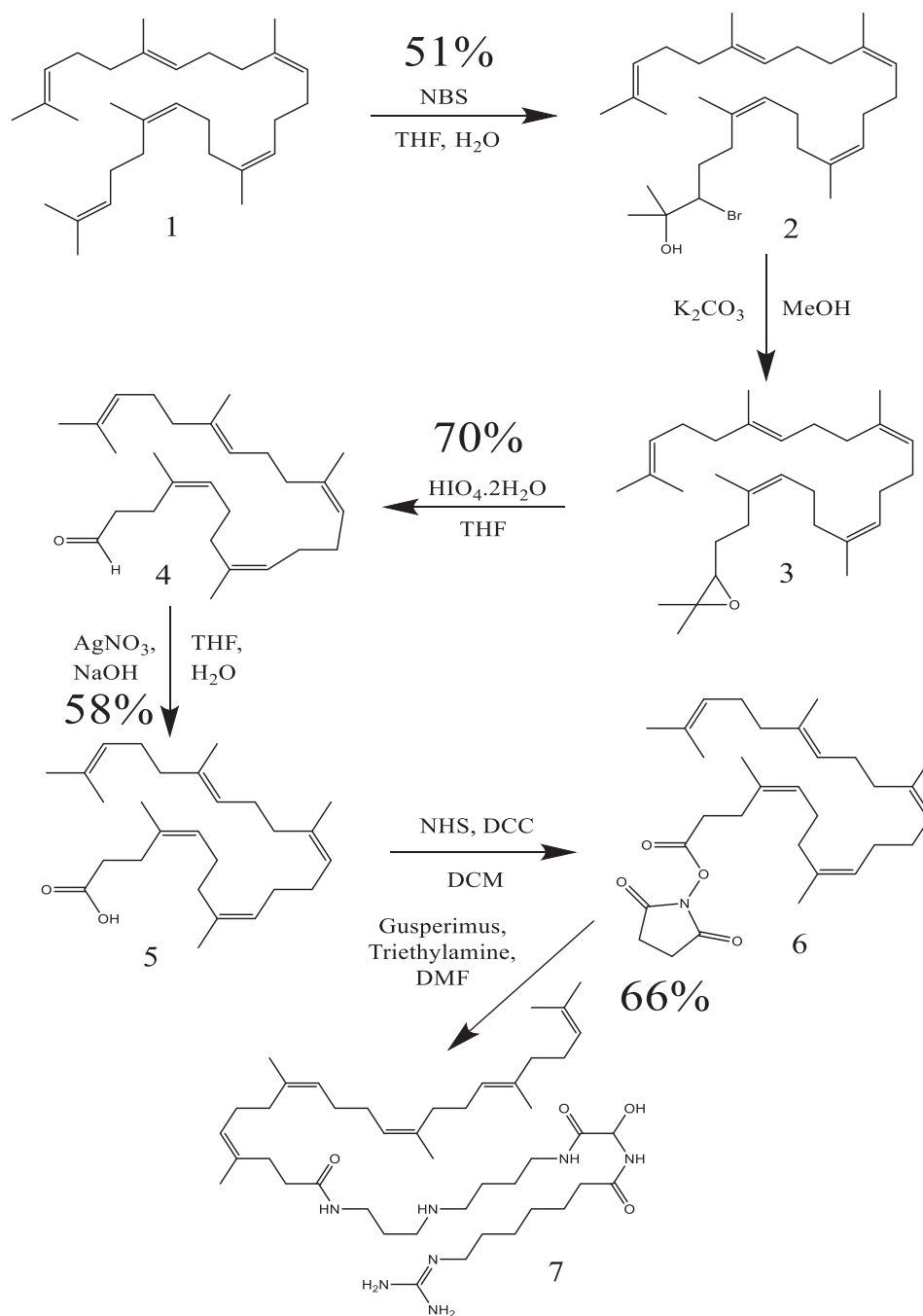


Fig. 1. Schematic representation of the synthesis of Sq-Gus bioconjugate (1) Squalene, (2) Sq-MBH, (3) Sq-Ep, (4) Sq-Ald, (5) Sq-COOH, (6) Sq-COO-NHS, (7) Sq-Gus bioconjugate. The quantities stated as a percentage were calculated based on the obtained yield.

of Sq-COOH (Fig. 3G) and Sq-Gus bioconjugate (Fig. 3I) present, in deuterated EtOH, low-intensity signals for their hydrophilic hydrogens (OH of the carboxylic acid group of Sq-COOH and amide, amine, and hydroxyl groups of Sq-Gus). The amphiphilic character of these compounds makes them adopt micelle like conformations in a moderately polar solvent like EtOH. This conformation results from interactions of the molecule lyophobic part with the solvent forming the shell. At the same time, the lyophilic parts of the molecules interact with themselves forming the nuclei with restricted mobility and short proton T_1 relaxation times producing low-intensity signals (Heald et al., 2002; Podo et al., 1973). In the case of the ^{13}C NMR spectrum of the Sq-Gus bioconjugate, it was not possible to observe all carbons of the molecule due to the low solubility of the conjugate in different deuterated solvents or

combination of them (data not shown). This together with especially short T_1 values for certain carbons decrease even more the already low sensibility of ^{13}C to the NMR experiment.

3.2. Use of RSM to transform Sq-Gus bioconjugate into NPs

Sq-Gus bioconjugate was transformed into NPs through the nanoprecipitation method using an ethanolic solution of the Sq-Gus bioconjugate (2 mg/mL), which was added to distilled water to form nanoassemblies. The optimal conditions for NPs preparation were established through an experimental design applying the RSM, which allowed the determination of factors influenced size, charge, and dispersity of the NPs. Treatments and responses obtained from the RSM

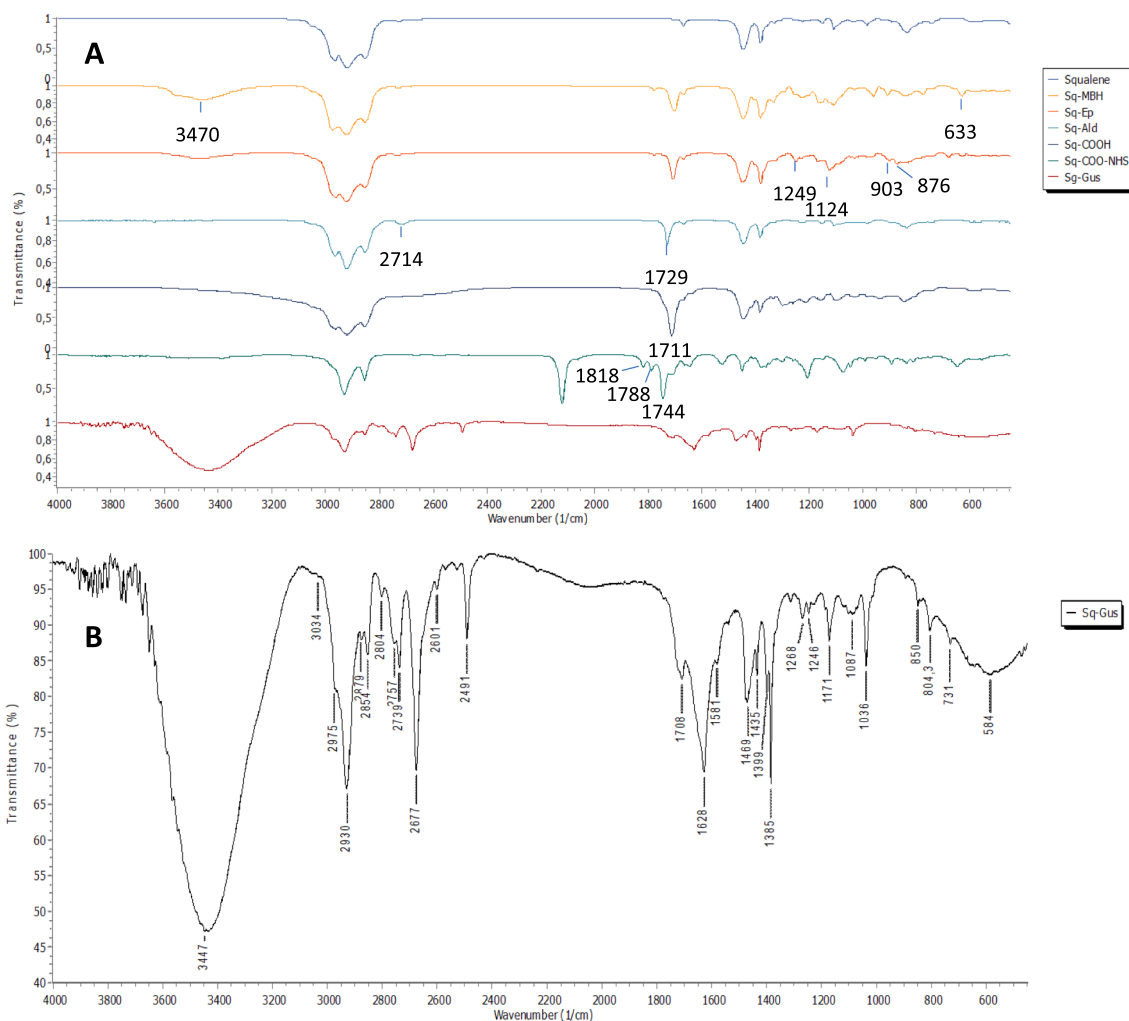


Fig. 2. Infrared spectra of the compounds involved in the Sq-Gus bioconjugate synthesis. (A) Stacked spectra of all synthesis products in the different reaction steps. (B) Infrared spectra of Sq-Gus bioconjugate.

design are shown in Table 2.

3.2.1. Effect of the volume of bioconjugate, the volume of water, and the stirring speed on NPs size

The Fig. 4A and Table S1 of the supplementary information show that any of the studied factors had a statistically significant effect on NPs size. Of these factors, stirring speed and the volume of the bioconjugate in EtOH had the most pronounced influence on the size compared to water volume and the interactions between factors. The stirring speed showed a negative effect on the size indicating that when it is increased, the NPs size decreases. The volume of the bioconjugate in ethanol, added to the water phase, had a positive effect on the NPs size, so an increase in the volume of the bioconjugate will enhance the NPs size. This indicates that an increase in the concentration of the bioconjugate implies an increase in the size of the NPs. The interaction between factors had a minor effect on NPs size.

3.2.2. Effect of the volume of bioconjugate, the volume of water, and the stirring speed on NPs charge

The surface charge of the NPs was most affected by the stirring speed (Fig. 4B and Table S2 of the supplementary information) with a negative effect on the variation of the z potential on NPs. The surface charge of the NPs became more negative when the stirring speed was enhanced. Therefore, increasing the stirring speed will enhance the stability of the NPs due to the increase of repulsive electrostatic interactions between

them. Neither the volume of the bioconjugate, nor the volume of water, or interactions between factors, had significant effects on NPs charge.

3.2.3. Effect of the volume of bioconjugate, the volume of water, and the stirring speed on NPs dispersity

The Fig. 4C and Table S3 of the supplementary information show that the \bar{D} of the NPs was affected at a higher degree by the volume of the bioconjugate with a negative effect on its variation. According to this, an increase in the concentration (Vol. bioconjugate) of the bioconjugate will produce NPs with a more uniform size or lower dispersity. Stirring speed and its interaction with the volume of the bioconjugate had contrary effects on \bar{D} but similar in magnitude. Therefore, an increase in the stirring speed and volume of the bioconjugate at the same time will produce smaller nanoparticles. It is to note that only the volume of the bioconjugate had a significant effect while the volume of water, the stirring speed and the interactions between factors showed a non-statistically significant effect on \bar{D} .

3.2.4. Optimization using the RSM

The previously studied response variables were normally distributed, with a constant variance, and independent of each other complying with the assumptions of the experimental design (Gutiérrez Pulido and de la Vara Salazar, 2008). According to the aforementioned, the obtained response surface (Fig. 4D) can precisely describe the behavior of the studied variables and could be used to predict the optimal values

Table 2

Treatments and responses obtained for the RSM design.

Treatment No.	Vol. Bioconjugate (μL)	Vol. water (mL)	Stirring speed (rpm)	Size (nm)	ζ (mV)	\mathcal{D}
1	400	3.5	535	134.5	-33.5	0.39
2	232	3.5	535	108.1	-33.5	0.57
3	300	2.0	800	114.6	-34.0	0.61
4	400	3.5	980	111.2	-32.3	0.45
5	400	3.5	535	114.8	-35.2	0.34
6	400	1.0	535	140.2	-30.0	0.08
7	500	2.0	800	118.1	-30.1	0.13
8	400	6.0	535	131.7	-32.6	0.33
9	500	2.0	270	145.2	-27.3	0.11
10	300	5.0	800	97.1	-36.5	0.75
11	500	5.0	800	124.5	-35.5	0.19
12	568	3.5	535	128.3	-28.0	0.16
13	300	2.0	270	120.7	-28.5	0.10
14	400	3.5	90	152.7	-26.4	0.30
15	500	5.0	270	155.0	-27.5	0.20
16	400	3.5	535	124.4	-31.8	0.24
17	300	5.0	270	112.7	-34.1	0.38

considering the interaction between the different responses. The obtained response surface is in terms of the desirability function (Table S4 of the supplementary information), which can take values between 0 and 1 and is defined according to the values set as the goal to obtain an optimal response. Based on the foregoing, we selected 140 nm for the particle size, -30 mV for ζ , and a minimum value for \mathcal{D} . The values established as a goal for each one of the response variables were chosen considering the observed behavior after the evaluation of the 17 treatments, where for treatment 6 the lowest dispersity was obtained (Table 2), and therefore the size and ζ for this treatment were chosen.

The conditions for nanoparticle preparation (Table 3) were obtained by optimization using the predicted values and the mathematical model of the RSM. As was expected, a variation in the responses was caused by slight changes in conditions used for nanoparticle preparation because of instrumental limitations as indicated in Table 3. A change in the obtained responses compared to the predicted values of 15.4%, 13.3%, and 11.1% for size, charge, and dispersity was obtained, respectively. Through TEM a spherical shape for the NPs was observed without internal organization (Fig. 4E and F), whose size agreed with DLS measurements (Table 3).

3.3. Colloidal stability of Sq-GusNPs

The colloidal stability for Sq-GusNPs was determined using a block experimental design in which the change in size and surface charge of the NPs was evaluated for 30 days at pH values of 4.5, 7.4, and 9.0 at 4 °C and 25 °C. The colloidal stability of Sq-GusNPs showed to be temperature and pH-dependent (Table S5 of the supplementary information). Higher stability could be obtained at 4 °C (Fig. 5A) since at this temperature at both pH 4.5 and 7.4, the NPs were stable for 30 days and at pH 9.0 for 20 days. When the NPs were stored at 25 °C at pH 7.4, the NPs were stable for 25 days while at pH 9.0 and 4.5 they were only stable for 15 and 10 days respectively (Fig. 5B). The highest stability was obtained when NPs were prepared at pH 7.4 at both temperatures. An increase in the magnitude of the NPs surface charge was observed when the pH was increased at both temperatures (Fig. 5C and D).

3.4. Uptake, toxicity, and efficacy in attenuating inflammatory responses of Sq-GusNPs in the U-937 cell line

3.4.1. Cell uptake of Sq-GusNPs

As gusperimus is efficacious in suppressing cells of the innate immunity (Perenyi et al., 2014) we evaluated cellular uptake, toxicity, and the anti-inflammatory capacity of Sq-GusNPs in the human U-937 cell line. Pinocytosis of Sq-GusNPs was followed by monitoring Nile-Red

labeled Sq-GusNPs uptake by the cells through flow cytometry, which was observed as a displacement towards the NR+ side (Fig. 6A). An increase of 6.1, 14.3, and 17.5 times the peak area was observed after exposing the cells to Nile-Red labeled NPs with respectively 1x, 2x, and 4x concentrations (Fig. 6B and C). As shown in Fig. 6C uptake was effective and concentration dependent. We were also able to visualize fluorescence in the cells (Fig. 6D) confirming NPs uptake.

3.4.2. Cytotoxicity of Sq-GusNPs

Cytotoxicity of Sq-GusNPs was tested through the determination of cell viability in U-937 monocytes with the two fluorophores PI and DiOC₆ through flow cytometry after exposure of the cells for 24 and 48 h to either free gusperimus, SqNPs, or Sq-GusNPs in equivalent concentrations (Fig. 7A and B). None of the treatments were toxic for the cells (Fig. 7C and D) in the times and ranges of concentrations evaluated which were 2.8 to 11.2 $\mu\text{g}/\text{mL}$ for gusperimus and squalene, and 5.6 to 22.3 $\mu\text{g}/\text{mL}$ for Sq-GusNPs.

3.4.3. Anti-inflammatory effect of Sq-GusNPs

To investigate the efficacy of Sq-GusNPs in attenuating inflammatory responses, U-937 monocytes were differentiated into macrophages by the addition of PMA (Haque et al., 2019). Subsequently, the cells were activated with LPS and 6 to 96 h later the anti-inflammatory capacity was studied by quantifying secretion of TNF α and IL-10. Cells were incubated with either Sq-GusNPs, free gusperimus, or SqNPs. Untreated cells and cells stimulated with LPS served as controls. After 6 h, Sq-GusNPs showed a clear anti-inflammatory effect. It significantly reduced LPS-induced TNF α secretion by the macrophages 2.7 times and IL-10 secretion 3.9 times compared with the control LPS ($p < 0.0001$) (Fig. 8A and B). There was no statistically significant difference between Sq-GusNPs and the other two treatments free gusperimus and SqNPs in the reduction of the inflammatory response. After 24, 48, and 72 h of exposition to LPS (Figure S5 of the supplementary information) there were less pronounced effects of gusperimus either as free or in encapsulated form, although only the treatment with Sq-GusNPs showed a tendency to the downregulation of both cytokines. After 96 h LPS exposition, Sq-GusNPs significantly reduced LPS-induced TNF α production 1.4 times compared to the control ($p < 0.005$) meanwhile free gusperimus, enhanced TNF α production 1.3 times higher than the LPS stimulated cells ($p < 0.005$) (Fig. 8A). Sq-GusNPs also reduced LPS-induced IL-10 secretion after 96 h ($p < 0.05$) (Fig. 8B).

4. Discussion

Here we present the design and characterization of a nano-encapsulation system for the immunosuppressive drug gusperimus using the platform originally proposed by Couvreur et al. (Couvreur et al., 2006). Gusperimus was bound covalently to squalene to obtain a bioconjugate or prodrug, which has the unique characteristic to self-assemble forming NPs in aqueous medium. The ability of the Sq-Gus bioconjugate to form nanoassemblies is due to its amphiphilic character where the squalene part provides the lyophobic moiety and the gusperimus the lyophilic one (Arpicco et al., 2016). The Sq-Gus bioconjugate chemical composition was confirmed by NMR analysis. The presence of the hydrophobic squalene moiety and the consequent increase in surface activity on the aqueous phase when the ethanolic solution of the bioconjugate was added are responsible of the formation of nanoassemblies (Couvreur et al., 2006). In the self-aggregation of the molecules occurring by lowering the surface tension, the interacting squalene moieties form the nuclei of the NPs (Desmaële et al., 2012). The homogeneous morphology and granulometry of the obtained NPs are the result of the more rigid conformation of the squalene derivatives as previously reported by Pogliani et al. (Pogliani et al., 1994). This nanoencapsulation procedure improved drug stability and availability as we demonstrated with stability and *in vitro* studies, respectively. Sq-GusNPs might also allow enhanced *in vivo* biodistribution of the active

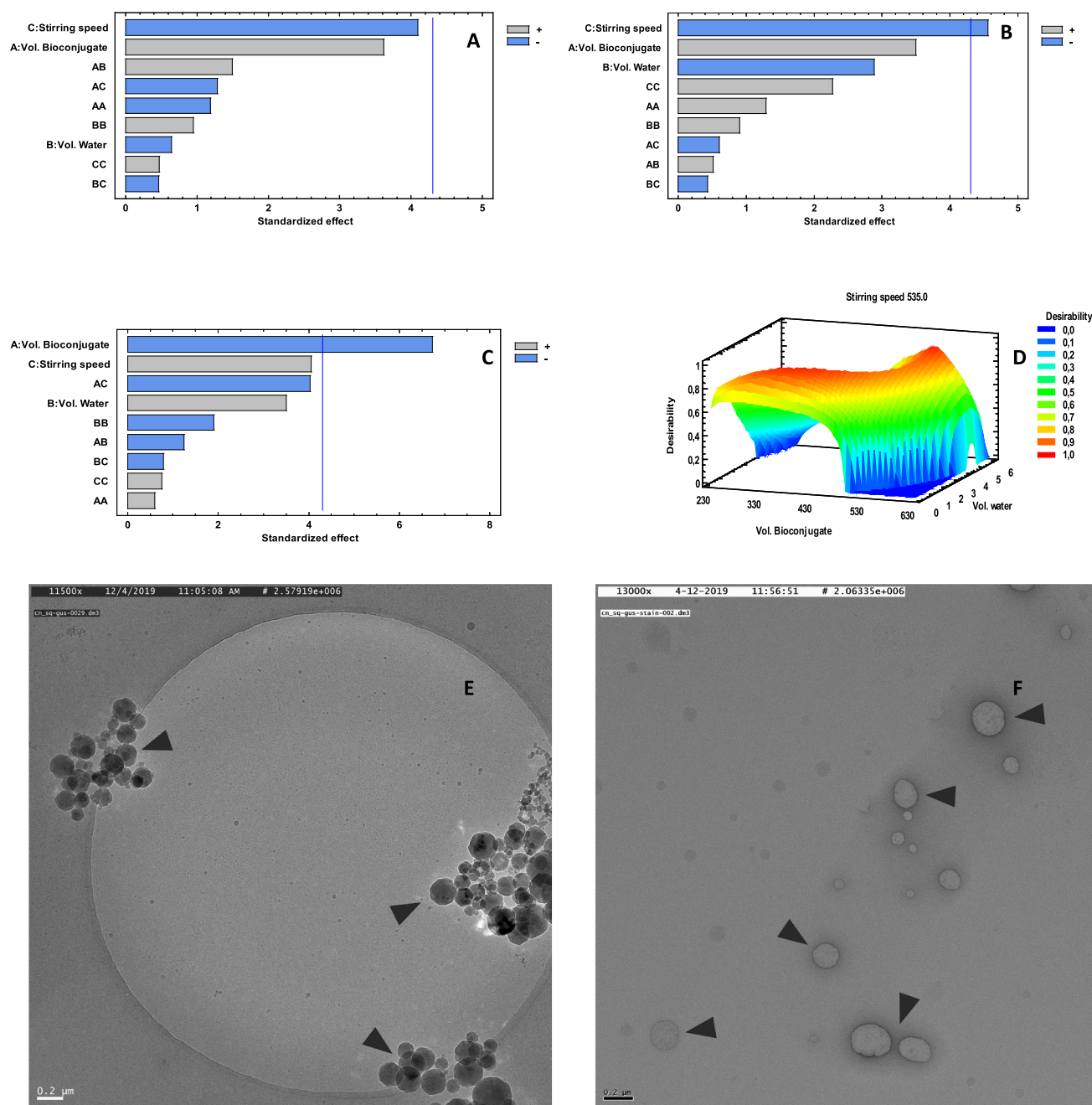


Fig. 4. Pareto diagrams for each one of the studied variables, response surface for Sq-GusNPs preparation through a CCD, and TEM images of the obtained NPs (A) Pareto diagram for Size. (B) Pareto diagram for ζ . (C) Pareto diagram for D . (D) Response surface obtained for the CCD experimental design. (E) Cryo-TEM images for Sq-GusNPs. (F) TEM images of Sq-GusNPs obtained after staining with a 2% of uranyl acetate solution. Arrowheads show the NPs; scale bars represent 200 nm.

Table 3

Predicted, used, and obtained values according to the RSM. NPs were prepared by triplicate and the responses are expressed as mean \pm standard deviation.

Factor	Predicted optimal point	Experimental optimal point	Response	Predicted value	Obtained response
Vol. Bioconjugate (µL)	380.24	380	Size (nm)	135.75	158.0 ± 48.8
Vol. Water (mL)	1.04	1	ζ (mV)	-30.00	-34.0 ± 0.7
Stirring speed (rpm)	510.83	500	D	0.09	0.1 ± 0.01

principle as it has been previously demonstrated for other squalene nanoparticulate delivery systems (Rouquette et al., 2019). The NPs were obtained through a bottom-up approach starting from the molecular components squalene and guserimus until the formation of the NPs. The bioconjugate was synthesized and characterized using

spectrometric techniques. NPs characteristics such as size, charge, dispersity, and stability were tuned and evaluated using the experimental design approaches of RSM and block design. For evaluation of the *in vitro* efficacy of Sq-GusNPs, we used the U-937 cell line and demonstrated its uptake, absence of toxicity, and anti-inflammatory capacity.

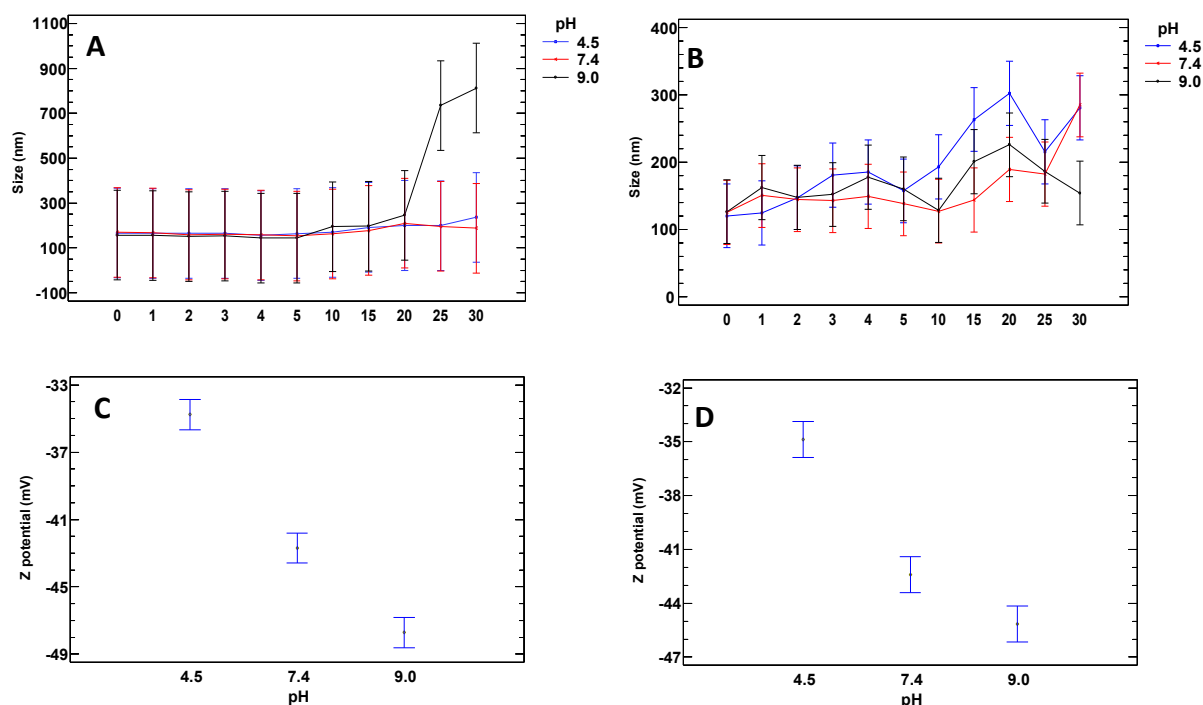


Fig. 5. Colloidal stability of Sq-GusNPs over time at different pH values evaluated using an experimental block design. (A) Size for Sq-GusNPs stored at 4 °C for 30 days. (B) Size for Sq-GusNPs stored at 25 °C for 30 days. (C) Z potential for Sq-GusNPs stored at 4 °C for 30 days. (D) Z potential for Sq-GusNPs stored at 25 °C for 30 days. The experiment included 11 blocks, was randomized, and for each temperature, this consisted of two replicas per block with a total of 66 runs.

By using FTIR and NMR we identified and characterized the different intermediate products from Sq-MBH until the formation of the Sq-Gus bioconjugate. In the reaction required to produce Sq-MBH, we observed selectivity of binding to one of the terminal olefinic bonds. This selectivity can be caused by the folded conformation of squalene in polar solvents induced by the water added to the squalene solution in THF during the first reaction step. In this folding phase, the internal olefinic bonds are protected from Br electrophilic addition due to intramolecular interactions of squalene (Desmaële et al., 2012). The squalene folding conformation in polar solvents has been previously demonstrated by Pogliani *et al.* (Pogliani et al., 1994), where, through NMR studies a diminution of relaxation times (T_1) in carbons located at the center of the squalene molecule was observed. The folding of the molecule is accompanied by an increased stiffness that goes from the end to the center of the squalene chain. This is an explanation for the availability of the olefinic extremes of the squalene chain for reacting with NBS to form the Sq-MBH due to its enhanced mobility. This is needed to obtain the subsequent derivatives and finally the Sq-Gus bioconjugate.

RSM is an experimental and analytical strategy that allows identification of the optimal operating conditions in a process allowing to set optimal values for one or several characteristics of the experimental unit (Gutiérrez Pulido and de la Vara Salazar, 2008) in this case the NPs. With the use of the parameters found with RSM (Table 2), Sq-GusNPs with an average size of 158 nm could be obtained. The NPs size distribution was uniform as was corroborated by a dispersity value of 0.1 (Danaei et al., 2018). The surface charge of the NPs was relatively high with an average value of -34.0 mV facilitating electrostatic repulsion forces that conferring them stability (Selvamani, 2019). This high surface charge of Sq-GusNPs influence features as uptake and intracellular trafficking (Gumustas et al., 2017). The gusperimus loading capacity of the NPs is 50.19%, as determined by the weight-contribution of the gusperimus to the Sq-Gus bioconjugate (Gaudin et al., 2016). However, the encapsulation efficiency, or conjugation efficiency, is 66% as determined by the yield obtained from the final reaction step in the synthesis process.

Colloidal stability is a measure for the long-term integrity of a

colloidal system as particles in the nanosized range tend to approach each other and form large aggregates due to interactions such as van der Waals forces (Selvamani, 2019). Colloidal stability can be reached through electrostatic or steric stabilization mechanisms (Myers, 1999). Our system showed to be very stable for at least 30 days (Fig. 5A) due to the high surface charge of the NPs, which was between -33 and -49 mV (Fig. 5C and D) at a wide range of pH values (Dosio et al., 2010). This finding provides insight into the stabilization mechanism of Sq-GusNPs, which is assumed to be due to electrostatic repulsion interactions (Gumustas et al., 2017).

Monocytes are innate immune cells and responsible for the first line of defense against pathogens with the potential to differentiate into macrophages or dendritic cells (Abbas et al., 2007). Monocytes are key players in modulating inflammation by producing pro-inflammatory cytokines such as IL-1 β , IL-6, and TNF- α as well as iNOS and anti-inflammatory cytokines as IL-10 and TGF- β 1. In this way, monocytes steer immune responses in both autoimmunity and graft rejection (Karlmark et al., 2012). Macrophages are more phagocytic cells and have some other, more specialized functions than monocytes and serve as cells responsible for antigen presentation, chemotaxis, and release of pro-inflammatory and anti-inflammatory cytokines (Bradlet, 2009). This was the reason to choose the U-937 cell line for this study as it is from human origin and because of its versatile properties to be used as monocytes or macrophages depending on the applied stimuli.

Sq-GusNPs was shown to be readily taken up by monocytes without any cytotoxic side-effect in the range between 5.6 and 22.3 μ g/mL. The Sq-GusNPs had a robust anti-inflammatory effect since both TNF α and IL-10 production were attenuated after LPS-stimulation at 6 and 96 h. A surprising observation was that not only gusperimus (Kälsch et al., 2006) but also squalene showed an anti-inflammatory effect at 6 h. This corroborates the findings of Ana Cárdeno *et al.* who studied the anti-inflammatory properties of squalene in neutrophils, monocytes, and macrophages *in vitro* (Cárdeno et al., 2015). The effects of squalene and gusperimus, however, were not as profound as that of Sq-GusNPs, which had a stronger tendency to attenuate both TNF α and IL-10 between 24 and 96 h (Fig. S5 of the supplementary information). In contrast,

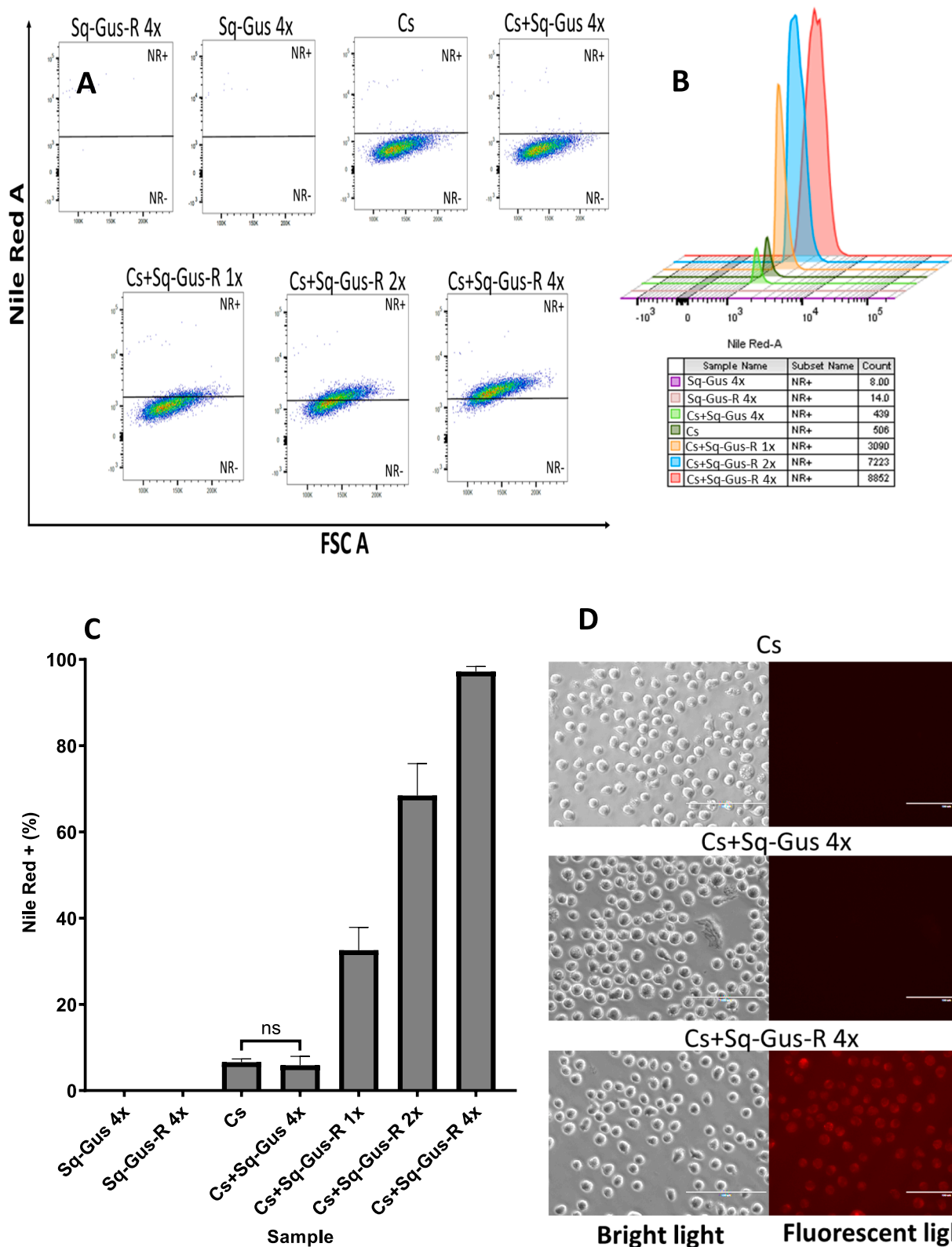


Fig. 6. Cellular uptake of Sq-GusNPs by monocytes after 3 h of incubation with Nile Red labeled NPs. (A) Dot plots obtained through flow cytometry for the applied treatments (NR+: Nile Red positive cells, NR-: Nile Red negative cells). (B) Stacked histograms showing the increment of fluorescent cells with the concentration of labeled Sq-GusNPs. (C) Cellular uptake of Sq-GusNPs expressed as Nile Red positive events for the applied treatments (ns: no significant difference). All treatments were statistically different from the control group (Cs) except the treatment Cs + Sq-GusNPs. (D) Micrographs obtained with bright light and fluorescent light for the cellular uptake experiment after 3 h of incubation at the highest evaluated concentration of Sq-GusNPs, scale bar represent 100 μ m. Sq-Gus 4x (no labeled NPs); Sq-Gus-R 4x (labeled Sq-GusNPs); Cs (cells without NPs); Cs + Sq-Gus 4x (cells treated with no labeled NPs); Cs + Sq-Gus-R (cells treated with labeled NPs). x is equivalent to 2.8 μ g/mL of free gusperimus. Comparisons were made using one-way ANOVA with Dunnett's post hoc test. Data represent mean values \pm SD of 5 independent experiments.

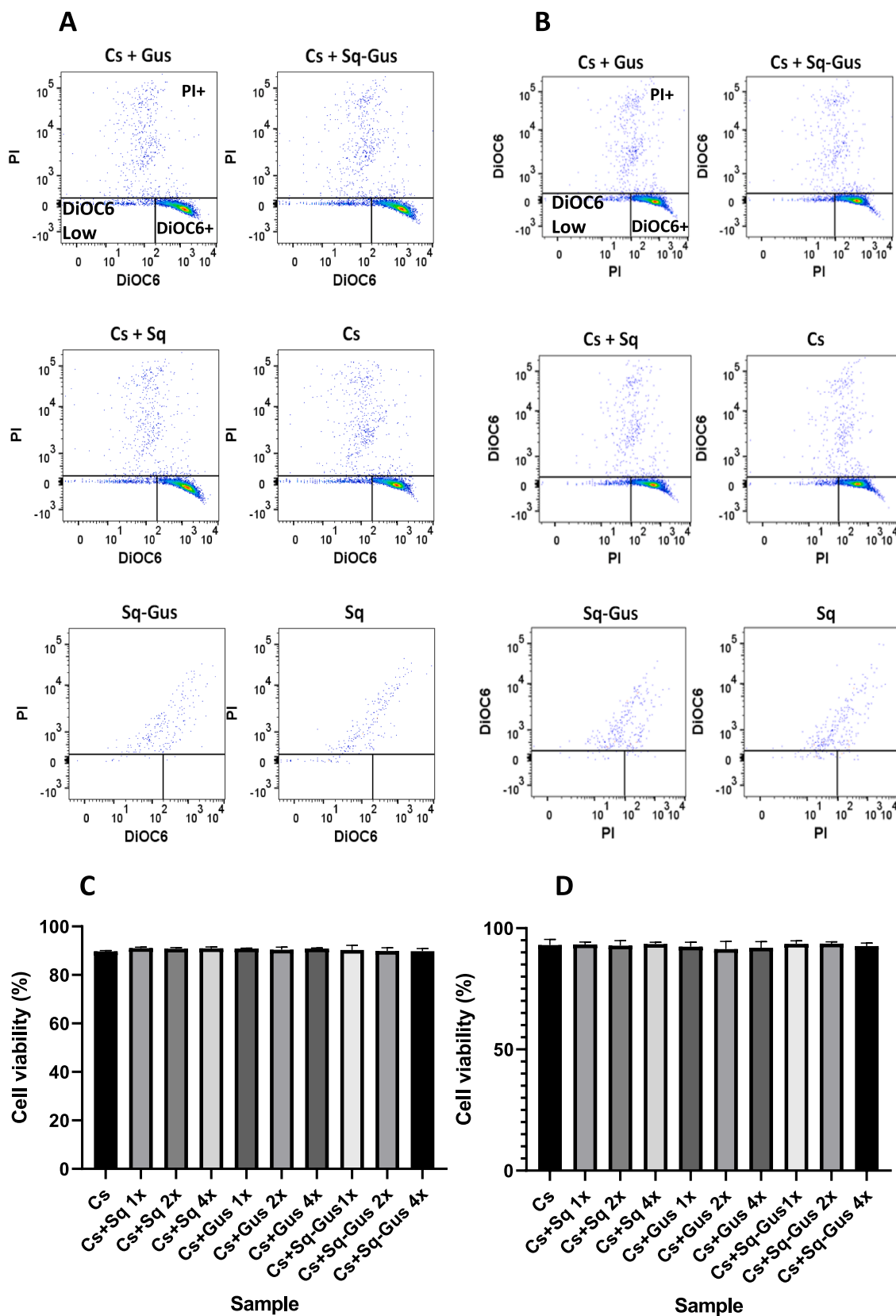


Fig. 7. Cytotoxicity of Sq-GusNPs in monocytes for 24 and 48 h. (A) Representative dot plots obtained through flow cytometry at 24 h for the treatments. (B) Representative dot plots obtained through flow cytometry at 48 h for the treatments. (PI+ superior box PI-positive cells, DiOC6 Low inferior left box, DiOC6 low absorption, DiOC6 + inferior right box DiOC6 positive cells). (C) Cell viability at 24 h for each treatment. (D) Cell viability at 48 h for each treatment. No statistical differences between the control (Cs) and the treatments for the evaluated time points were founded. Cs (Cells without any treatment); Cs+Sq-Gus (Cells treated with Sq-GusNPs); Cs+Gus (Cells treated with free gusperimus); Cs+Sq (Cells treated with SqNPs). x is equivalent to 2.8 µg/mL of free gusperimus or free squalene. Comparisons were made using one-way ANOVA with Dunnett's post hoc test. Data represent mean values ± SD of 3 independent experiments.

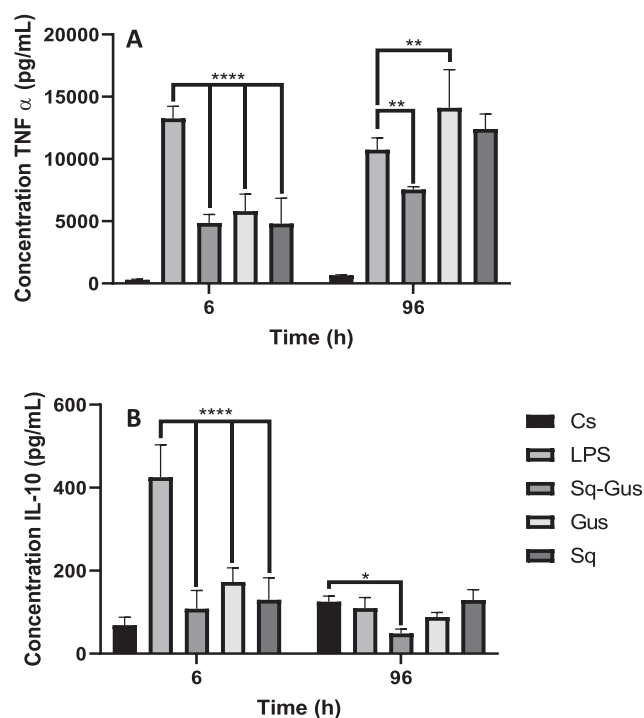


Fig. 8. Anti-inflammatory capacity of Sq-GusNPs. (A) TNF α production in LPS stimulated U-937 human macrophages at 6 and 96 h, only the treatment with Sq-GusNPs produced downregulation of the cytokine over time. (B) IL-10 production in LPS stimulated U-937 human macrophages after exposure to the different treatments, for the treatment with Sq-GusNPs was obtained the lowest concentration of the cytokine. Cs (Cells without any treatment); LPS (Cells treated with LPS); Sq-Gus (Cells treated with Sq-GusNPs); Gus (Cells treated with free gusperimus); Sq (Cells treated with SqNPs). Comparisons were made using two-way ANOVA with Tukey's post hoc test. Data represent mean values \pm SD of 3 independent experiments. $p < 0.0001$ (****); $p < 0.005$ (**); $p < 0.05$ (*).

squalene and gusperimus treatments showed no attenuation of the LPS-induced TNF α and IL-10 production over time demonstrating the specificity of Sq-GusNPs in attenuating inflammatory responses. We did observe, however, that treatment with free gusperimus caused a higher production of TNF α at 96 h. This can be explained by the high hydrophilic character of gusperimus which in the culture medium is unstable and hydrolyzed causing loss of its activity (Fujii et al., 1989). Further, it is oxidized to by-products that have shown cytotoxic effects on lymphocytes and leukemia cells (Fujii et al., 1989; Kerr et al., 1994). We showed that nanoencapsulation of gusperimus as Sq-GusNPs allows the induction of anti-inflammatory effects in the absence of toxicity and instability issues.

5. Conclusion

This study demonstrates that by using the squalenoylation platform (Couvreur et al., 2006) the immunosuppressive drug gusperimus can be nanoencapsulated as Sq-GusNPs, which has a profound influence on the bioactivity of gusperimus. These NPs are shown to be stable, have a high drug loading capacity, and *in vitro* a high uptake, lack of toxicity, and anti-inflammatory activity on both human monocytes and macrophages. This encapsulation system allows stabilization and controlled release of gusperimus, which was corroborated by the maintenance of gusperimus downregulatory effects over time for TNF α and IL-10 (Perenyi et al., 2014). These results suggest that the Sq-GusNPs are a promising therapeutic for the treatment of autoimmune diseases such as vasculitis, glomerulonephritis, systemic lupus erythematosus, rheumatoid arthritis, Crohn's disease, and management of graft rejection where

gusperimus has been shown to have high efficacy (Slobbe, 2012). Finally, further studies are necessary to determine important pharmacological characteristics and potential clinical applications involving the use of Sq-GusNPs as a therapeutic agent. These studies could include but are not limited to the determination of half-maximal inhibitory concentration (IC₅₀), internalization mechanisms involved in the uptake of the Sq-GusNPs, *in vivo* studies for determination of NPs biodistribution, residence time, and effect in different animal models of autoimmune diseases or organ transplantation.

CRedit authorship contribution statement

Carlos E. Navarro Chica: Conceptualization, Methodology, Investigation, Writing - original draft. **Bart J. de Haan:** Formal analysis, Resources. **M.M. Faas:** Writing - review & editing. **Alexandra M. Smink:** Formal analysis, Resources. **Ligia Sierra:** Writing - review & editing. **Paul de Vos:** Writing - review & editing, Supervision, Project administration, Funding acquisition. **Betty L. López:** Writing - review & editing, Supervision, Project administration, Funding acquisition.

Declaration of Competing Interest

The authors declare that they have no known competing financial interests or personal relationships that could have appeared to influence the work reported in this paper.

Acknowledgments

This work was supported by the Abel Tasman Talent Program of the University of Groningen and the COLCIENCIAS project "Preparation and characterization of Gusperimus nanocarriers with potential application in the process of implantation of cellular islets for the treatment of type 1 diabetes mellitus" contract 747-2018, N^o 111580763077.

Data availability

Datasets generated during and/or analyzed during the current study are in the supplementary data of this paper. Additional datasets are available from the corresponding author upon reasonable request.

Appendix A. Supplementary data

Supplementary data to this article can be found online at <https://doi.org/10.1016/j.ijpharm.2020.119893>.

References

- Abbas, A.K., Lichtman, A.H., Pillai, S., 2007. *Cellular and molecular immunology*, 6th ed. Saunders Elsevier.
- Arpico, S., Battaglia, L., Brusa, P., Cavalli, R., Chirio, D., Dosio, F., Gallarate, M., Milla, P., Peira, E., Rocco, F., Sapino, S., Stella, B., Ugazio, F., Ceruti, M., 2016. Recent studies on the delivery of hydrophilic drugs in nanoparticulate systems. *J. Drug Deliv. Sci. Technol.* 32, 298–312. <https://doi.org/10.1016/j.jddst.2015.09.004>.
- B.Kaufman, D., F.Gores, P., Kelley, S., M.Grasela, D., G. Nadler, S., EleanorRamos, 1996. 15-deoxyspergualin: Immunotherapy in solid organ and cellular transplantation. *Transplant. Rev.* 10, 160–174. [https://doi.org/https://doi.org/10.1016/S0955-470X\(96\)80025-5](https://doi.org/https://doi.org/10.1016/S0955-470X(96)80025-5).
- Barreras-Urbina, C.G., Ramírez-Wong, B., López-Ahumada, G.A., Burruel-Ibarra, S.E., Martínez-Cruz, O., Tapia-Hernández, J.A., Rodríguez Félix, F., 2016. Nano- and Micro-Particles by Nanoprecipitation: Possible Application in the Food and Agricultural Industries. *Int. J. Food Prop.* 19, 1912–1923. <https://doi.org/10.1080/10942912.2015.1089279>.
- Bradlet, S., 2009. Conversion of the U937 Monocyte into "Macrophage-Like" Populations Exhibiting M1 or M2 Characteristics. Wright State University, Browns. all Theses Diss.
- Cárdeno, A., Aparicio-Soto, M., Montserrat-de la Paz, S., Bermudez, B., Muriána, F.J.G., Alarcón-de-la-Lastra, C., 2015. Squalene targets pro- and anti-inflammatory mediators and pathways to modulate over-activation of neutrophils, monocytes and macrophages. *J. Funct. Foods* 14, 779–790. <https://doi.org/10.1016/j.jff.2015.03.009>.

- Ceruti, M., Balliano, G., Viola, F., Cattel, L., Gerst, N., Schuber, F., 1987. Synthesis and biological activity of azasqualenes, bis-azasqualenes and derivatives. *Eur. J. Med. Chem.* 22, 199–208. [https://doi.org/10.1016/0223-5234\(87\)90050-X](https://doi.org/10.1016/0223-5234(87)90050-X).
- Ceruti, M., Balliano, G., Viola, F., Groso, G., Rocco, F., Cattel, L., 1992. 2,3-Epoxy-10-aza-10,11-dihydrosqualene, a High-Energy Intermediate Analogue Inhibitor of 2,3-Oxidosqualene Cyclase. *J. Med. Chem.* 35, 3050–3058. <https://doi.org/10.1021/jm00094a020>.
- Clayden, J., Greeves, N., Warren, S., 2012. *Organic Chemistry, Second. ed.* Oxford University Press Inc.
- Clayton, K.N., Salameh, J.W., Wereley, S.T., Kinzer-Ursem, T.L., 2016. Physical characterization of nanoparticle size and surface modification using particle scattering diffusometry. *Biomicrofluidics* 10, 1–14. <https://doi.org/10.1063/1.4962992>.
- Conversion of Carboxylic acids to amides using DCC as an activating agent - Chemistry LibreTexts [WWW Document], n.d. URL [https://chem.libretexts.org/Bookshelves/Organic_Chemistry/Supplemental_Modules_\(Organic_Chemistry\)/Carboxylic_Acids/Reactivity_of_Carboxylic_Acids/Conversion_of_Carboxylic_acids_to_amides_using_DCC_as_an_activating_agent](https://chem.libretexts.org/Bookshelves/Organic_Chemistry/Supplemental_Modules_(Organic_Chemistry)/Carboxylic_Acids/Reactivity_of_Carboxylic_Acids/Conversion_of_Carboxylic_acids_to_amides_using_DCC_as_an_activating_agent) (accessed 10.30.19).
- Couvreur, P., Lakkireddy, Harivardhan, R., Dosio, F., Stella, B., Cattel, L., 2009. Nanoparticles of therapeutic agents having low water solubility, Patent WO2009071850A2.
- Couvreur, P., Stella, B., Harivardhan Reddy, L., Hillaireau, H., Dubernet, C., Desmaële, D., Lepêtre-Mouelhi, S., Rocco, F., Dereuddre-Bosquet, N., Clayette, P., Rosilio, V., Marsaud, V., Renoir, J.M., Cattel, L., 2006. Squalenol nanomedicines as potential therapeutics. *Nano Lett.* 6, 2544–2548. <https://doi.org/10.1021/nl061942q>.
- Danaei, M., Dehghankhold, M., Ataei, S., Hasanazadeh Davarani, F., Javanmard, R., Dokhani, A., Khorasani, S., Mozafari, M.R., 2018. Impact of particle size and polydispersity index on the clinical applications of lipidic nanocarrier systems. *Pharmaceutics* 10, 1–17. <https://doi.org/10.3390/pharmaceutics10020057>.
- Desmaële, D., Gref, R., Couvreur, P., 2012. Squalenoylation: A generic platform for nanoparticulate drug delivery. *J. Control. Release* 161, 609–618. <https://doi.org/10.1016/j.jconrel.2011.07.038>.
- Dosio, F., Reddy, L.H., Ferrero, A., Stella, B., Cattel, L., Couvreur, P., 2010. Novel nanoassemblies composed of squalenoyl-paclitaxel derivatives: Synthesis, characterization, and biological evaluation. *Bioconjug. Chem.* 21, 1349–1361. <https://doi.org/10.1021/bc100154g>.
- Ebrahiminezhad, A., Ghasemi, Y., Rasoul-Amini, S., Barar, J., Davaran, S., 2012. Impact of amino acid coating on the synthesis and characteristics of iron-oxide nanoparticles (IONs). *Bull. Korean Chem. Soc.* 33, 3957–3962. <https://doi.org/10.5012/bkcs.2012.33.12.3957>.
- Feng, J., Lepetre-Mouelhi, S., Couvreur, P., 2017. Design, preparation and characterization of modular squalene-based nanosystems for controlled drug release. *Curr. Top. Med. Chem.* 17, 2849–2865. <https://doi.org/10.2174/156802661766617071917128>.
- Fujii, H., Takada, T., Nemoto, K., Abe, F., Fujii, A., Takeuchi, T., 1989. In vitro immunosuppressive properties of spergualins to murine T cell response. *J. Antibiot. (Tokyo)* 42, 788–794. <https://doi.org/10.7164/antibiotics.42.788>.
- Gaudin, A., Song, E., King, A.R., Saucier-Sawyer, J.K., Bindra, R., Desmaële, D., Couvreur, P., Saltzman, W.M., 2016. PEGylated squalenoyl-gemcitabine nanoparticles for the treatment of glioblastoma. *Biomaterials* 105, 136–144. <https://doi.org/10.1016/j.biomaterials.2016.07.037>.
- Gumustas, M., Sengel-Turk, C.T., Gumustas, A., Ozkan, S.A., Uslu, B., 2017. Effect of Polymer-Based Nanoparticles on the Assay of Antimicrobial Drug Delivery Systems, Multifunctional Systems for Combined Delivery, Biosensing and Diagnostics. Elsevier Inc. <https://doi.org/10.1016/b978-0-323-52725-5.00005-8>.
- Gusperimus | C17H37N7O3 - PubChem [WWW Document], n.d. URL <https://pubchem.ncbi.nlm.nih.gov/compound/55362#section=Experimental-Properties> (accessed 10.23.19).
- Gutiérrez Pulido, H., de la Vara Salazar, R., 2008. *Análisis y diseño de experimentos, Segunda. ed.* McGRAW-HILL/INTERAMERICANA.
- Haq, M.A., Jantan, I., Harikrishnan, H., Ghazalee, S., 2019. Standardized extract of Zingiber zerumbet suppresses LPS-induced pro-inflammatory responses through NF- κ B, MAPK and PI3K-Akt signaling pathways in U937 macrophages. *Phytomedicine* 54, 195–205. <https://doi.org/10.1016/j.phymed.2018.09.183>.
- Heald, C.R., Stolnik, S., Kujawinski, K.S., Matteis, C. De, Garnett, M.C., Illum, L., Davis, S.S., Purkiss, S.C., Barlow, R.J., Gellert, P.R., 2002. Poly(lactic acid)-Poly(ethylene oxide) (PLA-PEG) Nanoparticles: NMR Studies of the Central Solidlike PLA Core and the Liquid PEG Corona. *Langmuir* 18, 3669–3675. <https://doi.org/10.1021/la011393y>.
- Kälsch, A.I., Schmitt, W.H., Breedijk, A., Marinaki, S., Weigerding, S., Nebe, T.C., Nemoto, K., Van Der Woude, F.J., Yard, B.A., Birck, R., 2006. In vivo effects of cyclic administration of 15-deoxyspergualin on leucocyte function in patients with Wegener's granulomatosis. *Clin. Exp. Immunol.* 146, 455–462. <https://doi.org/10.1111/j.1365-2249.2006.03231.x>.
- Karlmark, K., Tacke, F., Dunay, I., 2012. Monocytes in health and disease — Minireview. *Eur. J. Microbiol. Immunol.* 2, 97–102. <https://doi.org/10.1556/eujmi.2.2012.2.1>.
- Kawada, M., Masuda, T., Ishizuka, M., Takeuchi, T., 2002. 15-Deoxyspergualin inhibits Akt kinase activation and phosphatidylcholine synthesis. *J. Biol. Chem.* 277, 27765–27771. <https://doi.org/10.1074/jbc.M200318200>.
- Kerr, P.G., Ntkolic-Paterson, D.J., Lan, H.Y., Tesch, G., Rainone, S., Atkins, R.C., 1994. Deoxyspergualin suppresses local macrophage proliferation in rat renal allograft rejection. *Transplantation* 58, 596–601. <https://doi.org/10.1097/00007890-199409150-00012>.
- Myers, D., 1999. Surfaces, interfaces, and colloids: Principles and Applications, Second. ed. John Wiley & Sons, Inc. <https://doi.org/10.1002/0471234990>.
- Nagarkatti, J.P., Ashley, K.R., 1973. Periodic acid cleavage of epoxides in aqueous medium. *Tetrahedron Lett.* 14, 4599–4600. [https://doi.org/10.1016/S0040-4039\(01\)87286-5](https://doi.org/10.1016/S0040-4039(01)87286-5).
- Nishimura, K., Ohki, Y., Fukuchi-Shimogori, T., Sakata, K., Saiga, K., Beppu, T., Shirahata, A., Kashiwagi, K., Igarashi, K., 2002. Inhibition of cell growth through inactivation of eukaryotic translation initiation factor 5A (eIF5A) by deoxyspergualin. *Biochem. J.* 363, 761–768. <https://doi.org/10.1042/0264-6021:3630761>.
- Odaka, C., Toyoda, E., Nemoto, K., 1998. Immunosuppressant deoxyspergualin induces apoptotic cell death in dividing cells. *Immunology* 95, 370–376. <https://doi.org/10.1046/j.1365-2567.1998.00606.x>.
- Perenyi, M., Jayne, D.R.W., Floßmann, O., 2014. Gusperimus: Immunological mechanism and clinical applications. *Rheumatol. (United Kingdom)* 53, 1732–1741. <https://doi.org/10.1093/rheumatology/ket451>.
- Podo, F., Ray, A., Nemethy, G., 1973. Structure and hydration of nonionic detergent micelles. High resolution nuclear magnetic resonance study. *J. Am. Chem. Soc.* 95, 6164–6171. <https://doi.org/10.1021/ja00800a003>.
- Pogliani, L., Ceruti, M., Ricchiardi, G., Viterbo, D., 1994. An NMR and molecular mechanics study of squalene and squalene derivatives. *Chem. Phys. Lipids* 70, 21–34. [https://doi.org/10.1016/0009-3084\(94\)90044-2](https://doi.org/10.1016/0009-3084(94)90044-2).
- Rosenberg, M., Azevedo, N.F., Ivask, A., 2019. Propidium iodide staining underestimates viability of adherent bacterial cells. *Sci. Rep.* 9, 1–12. <https://doi.org/10.1038/s41598-019-42906-3>.
- Rouquette, M., Lepetre-Mouelhi, S., Dufrancois, O., Yang, X., Mouglin, J., Pieters, G., Garcia-Argote, S., IJzerman, A.P., Couvreur, P., 2019. Squalene-adenosine nanoparticles: Ligands of adenosine receptors or adenosine prodrg? *J. Pharmacol. Exp. Ther.* 369, 144–151. <https://doi.org/10.1124/jpet.118.254961>.
- Selvamani, V., 2019. Stability Studies on Nanomaterials Used in Drugs, Characterization and Biology of Nanomaterials for Drug Delivery. Elsevier Inc. <https://doi.org/10.1016/b978-0-12-814031-4.00015-5>.
- Sen, S.E., Prestwich, G.D., 1989. Trisnorsqualene alcohol, a potent inhibitor of vertebrate squalene epoxidase. *J. Am. Chem. Soc.* 111, 1508–1510. <https://doi.org/10.1021/ja00186a062>.
- Shapiro, H.M., 2000. Membrane potential estimation by flow cytometry. *Methods* 21, 271–279. <https://doi.org/10.1006/meth.2000.1007>.
- Silverstein, R.M., Webster, F.X., Kiemle, D.J., 2005. *Spectrometric identification of organic compounds, 7th ed.* Jhon Wiley and Sons Inc.
- Slobbe, L., 2012. Drugs that act on the immune system: Immunosuppressive and immunostimulatory drugs, 1st ed, Side Effects of Drugs Annual. Elsevier B.V. <https://doi.org/10.1016/B978-0-444-59499-9.00038-6>.
- Takeuchi, T., Iinuma, H., Kunimoto, S., Masuda, T., Ishizuka, M., Takeuchi, M., Hamada, M., Naganawa, H., Kondo, S., Umezawa, H., 1981. A new antitumor antibiotic, spergualin: Isolation and antitumor activity. *J. Antibiot. (Tokyo)* 34, 1619–1621. <https://doi.org/10.7164/antibiotics.34.1619>.
- Thangaraj, U.D., Rajagantham, M., Govindarajulu, K., Arulsamy, J.P., 2017. Synthesis, crystal structure and vibrational spectral analysis of guanidinium hydrogen L-aspartate single crystal. *J. Phys. Sci.* 28, 27–47. <https://doi.org/10.21315/jps2017.28.1.3>.
- Wang, L., Gao, X., Gao, P., Deng, W., Yu, P., Ma, J., Guo, J., Wang, X., Cheng, H., Zhang, C., Yu, C., Ma, X., Bingfeng, L.V., Lu, Y., Shi, T., Ma, D., 2006. Cell-based screening and validation of human novel genes associated with cell viability. *J. Biomol. Screen.* 11, 369–376. <https://doi.org/10.1177/1087057106286654>.
- Zhao, C.X., He, L., Qiao, S.Z., Middelberg, A.P.J., 2011. Nanoparticle synthesis in microreactors. *Chem. Eng. Sci.* 66, 1463–1479. <https://doi.org/10.1016/j.ces.2010.08.039>.